ACSNANO
www.acsnano.org
ARTICLE

Highly Sensitive and Quick Detection of Acute Myocardial Infarction Biomarkers Using In_2O_3 Nanoribbon Biosensors Fabricated Using Shadow Masks

Qingzhou Liu,[†] Noppadol Aroonyadet,[‡] Yan Song,[§] Xiaoli Wang,[‡] Xuan Cao,[†] Yihang Liu,[‡] Sen Cong,[‡] Fanqi Wu,[‡] Mark E. Thompson,[*,†,§] and Chongwu Zhou[*,†,‡]

[†]Mork Family Department of Chemical Engineering and Materials Science, [‡]Ming Hsieh Department of Electrical Engineering, and [§]Department of Chemistry, University of Southern California, Los Angeles, California 90089, United States

Supporting Information

ABSTRACT: We demonstrate a scalable and facile lithography-free method for fabricating highly uniform and sensitive In_2O_3 nanoribbon biosensor arrays. Fabrication with shadow masks as the patterning method instead of conventional lithography provides low-cost, time-efficient, and high-throughput In_2O_3 nanoribbon biosensors without photoresist contamination. Combined with electronic enzyme-linked immunosorbent assay for signal amplification, the In_2O_3 nanoribbon biosensor arrays are optimized for early, quick, and quantitative detection of cardiac biomarkers in diagnosis of acute myocardial infarction (AMI). Cardiac troponin I (cTnI), creatine kinase MB (CK-MB), and B-type natriuretic peptide (BNP) are commonly associated with heart attack and heart failure and have been selected as the target biomarkers here. Our approach can detect label-free biomarkers for concentrations down to 1 pg/mL (cTnI), 0.1 ng/mL (CK-MB), and 10 pg/mL (BNP), all of which are much lower than clinically relevant cutoff concentrations. The sample collection to result time is only 45 min, and we have further demonstrated the reusability of the sensors. With the demonstrated sensitivity, quick turnaround time, and reusability, the In_2O_3 nanoribbon biosensors have shown great potential toward clinical tests for early and quick diagnosis of AMI.

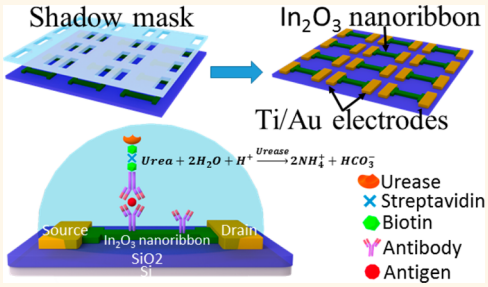

KEYWORDS: *biosensor, indium oxide semiconductor, field-effect transistor, shadow mask fabrication, electronic ELISA, acute myocardial infarction diagnosis*

Every year, about 5 million patients visit the emergency department because of chest pain symptoms, but only 10% of these patients experience acute myocardial infarction (AMI).[1] If an initial electrocardiogram (ECG) assessment at the emergency department reveals a ST-segment elevation, the patient is placed at high risk for AMI, or heart attack, and the established medical procedures are administered to the patient. However, the ECG sensitivity may be as low as 50%,[2−5] and patients who show no ST elevation can still be at high risk for unstable angina or non-ST-segment elevation AMI. For this reason, cardiac biomarkers have become increasingly important for swift risk stratifying and diagnosing patients who may still need immediate treatment.

The effectiveness of the biomarkers to properly diagnose and triage chest pain patients is based on several factors. First, the test turnaround time should be short because early treatment of myocardial infarction is crucial to recovery. The American Heart Association has stated a recommended turnaround time of 60 min and a preferred turnaround time of 30 min from sample collection to result reporting.[6] Second, obtaining the trend in the cardiac biomarker concentration in the hours after a patient's arrival is a crucial addition to the initial cardiac biomarker reading for accurate diagnosis. Current biomarker trends are collected through serial biomarker readings, such as testing at 0, 30, 60, and 90 min after patient arrival at the emergency department.[7] Such fast turnaround times are difficult to achieve in a central laboratory setting and are often aided by a point-of-care (POC) device.[8] Additionally, multiple cardiac biomarker testing may improve the diagnosis process of heart attack over single biomarker testing.[9] The National Academy of Clinical Biochemistry has recommended testing for an early biomarker that elevates within the first 6 h of chest pain in conjuncture with an AMI-specific biomarker that is increased in the blood even after 6−9 h.[10] Point-of-care

Received: August 1, 2016
Accepted: October 21, 2016

DOI: 10.1021/acsnano.6b05171
ACS Nano XXXX, XXX, XXX−XXX

platforms are ideal for multiple cardiac biomarker testing with fast turnaround times, but current POC devices lack the good sensitivity and high specificity of central laboratory biomarker testing.[11] For POC devices to more effectively aid rapid decision making in both the emergency department and in the field, there is a need for further investigation of emerging sensor technology in order to bridge the performance gap between the POC device and central laboratory testing for cardiac biomarkers.

Great progress was made with silicon nanoribbons fabricated using top-down methods, which have been shown to be highly sensitive, scalable, and uniform.[12,13] However, the fabrication process is rather complicated; for example, it needs oxidation, photolithography, and wet etching. Moreover, Si nanoribbon devices usually require silicon-on-insulator wafers, which are expensive. Semiconducting metal-oxide-based biosensors have several advantages, such as the use of low-cost Si/SiO_2 wafers and the ease of fabrication when compared to silicon-based biosensors. By using the shadow mask fabrication method, we can choose many kinds of substrates, such as Si/SiO_2 wafers, glass, or even plastic substrates; however, some of the commercially available plastic substrates may not be compatible with the photoresist baking step used for photolithography, which would make the shadow mask approach advantageous. Furthermore, in comparison with multiple-step cleanroom fabrication, fabrication with shadow masks is cost-efficient, highly reliable, photolithography-free, room-temperature processing and can be performed without using a cleanroom. In addition, nowadays shadow masks can be obtained rather easily by submitting the mask design to commercial service providers (such as Photo Sciences Inc.), and the size of the shadow masks can be as large as 6 in., making wafer-scale fabrication very easy.

Indium oxide (In_2O_3) field-effect transistors (FETs) have been shown to be real-time and label-free detectors with superb signal-to-noise ratio and the potential for integrated multiplexing.[14−18] The quick response time makes the In_2O_3 nanoribbon sensors especially advantageous for analyzing the first blood-drawn sample, from which rapid decisions can be made for the patients' treatment. The small device-to-device variation demonstrated previously[14] can provide good statistical confidence for calibrating cardiac biomarker concentrations. Furthermore, In_2O_3 nanoribbon sensors can provide quantitative analysis for a large detectable concentration range spanning at least 4 orders of magnitude and a detection limit in the picogram per milliliter range.[14] This sensitivity can help to differentiate biomarker changes at each serial reading. Due to the electronic sensing, the final product enjoys facile interface and compactness while having the capability to integrate with other microfluidic and electronic functional groups, such as wireless data output.[19] These properties make In_2O_3 nanoribbon sensors well-suited for analyzing medical conditions such as heart attack that require urgent POC medical attention. However, in our previous work, two steps of photolithography were performed to produce In_2O_3 nanoribbon sensors, which may increase the cost and the fabrication time significantly. It is therefore highly important to develop a low-cost, time-efficient, and scalable lithography-free process to produce In_2O_3 nanoribbon FETs, which may generate broad impact to applications such as chemical sensing,[20−22] protein detection,[23,24] cancer diagnosis and prognosis,[25] infectious disease diagnosis, biomedical research,[12,26] and even thin film transistors for displays and macro electronics.

Here, we present a lithography-free process for the fabrication of highly sensitive and scalable FET-based In_2O_3 nanoribbon biosensors. The nanoribbons are prepared by sputter-coating In_2O_3 through a shadow mask onto a substrate and have a ribbon-like cross section of ~16 nm in thickness, 25 μm in width, and 500 μm in length, followed by metal electrode deposition through another shadow mask. The devices fabricated by shadow masks show good electrical performance in both ambient and aqueous environment, with the surfaces never exposed to undesirable chemicals like photoresist or e-beam resist. In addition, In_2O_3 nanoribbon devices also show good performance in pH sensing experiments. Through all the sensing experiments, we have demonstrated that In_2O_3 nanoribbon biosensors fabricated using shadow masks can be used to quantitatively detect three cardiac biomarkers within the concentrations relevant to clinical diagnosis with the turnaround time ~45 min. We further demonstrated tests using spiked cardiac biomarkers in diluted human blood. Lastly, by first applying regeneration buffer to the used sensor surface to antibond the antigen−antibody conjugation and then repeating the sensing experiments, we demonstrated the reusability of the In_2O_3 nanoribbon biosensors with very small variation of each sensing result.

RESULTS AND DISCUSSION

Indium oxide as an active channel material has been shown to function effectively in the biosensing platform. In this work, we fabricate the nanoribbon devices using a shadow mask technique on 3 in. silicon substrates covered with 500 nm thick silicon oxide. Figure 1a shows the schematic diagram depicting the fabrication process. The first shadow mask step defines the dimension and position of the nanoribbons by

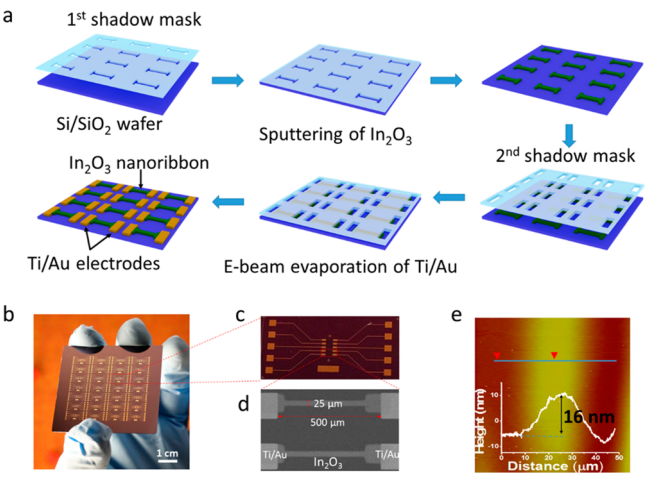

Figure 1. In_2O_3 FET-based biosensors fabricated by a shadow mask. (a) Schematic illustration of the lithography-free biosensor fabrication procedure. The first layer shadow mask was attached onto the SiO_2/Si substrate. In_2O_3 thin films were deposited by RF sputtering. After the first layer shadow mask was detached and replaced with the second layer, 1/50 nm Ti/Au was deposited to the surface by e-beam evaporation. By removing the second layer shadow mask, we obtained a FET-based biosensor with pristine surface. (b) Optical image of a 3 in. wafer of an In_2O_3 nanoribbon biosensor. (c) Magnified image of a biosensor chip with five nanoribbon devices in one group. (d) SEM image of two In_2O_3 nanoribbon devices (L = 500 μm, W = 25 μm). (e) Atomic force microscopy image of a ~16 nm thick In_2O_3 nanoribbon.

DOI: 10.1021/acsnano.6b05171
ACS Nano XXXX, XXX, XXX−XXX

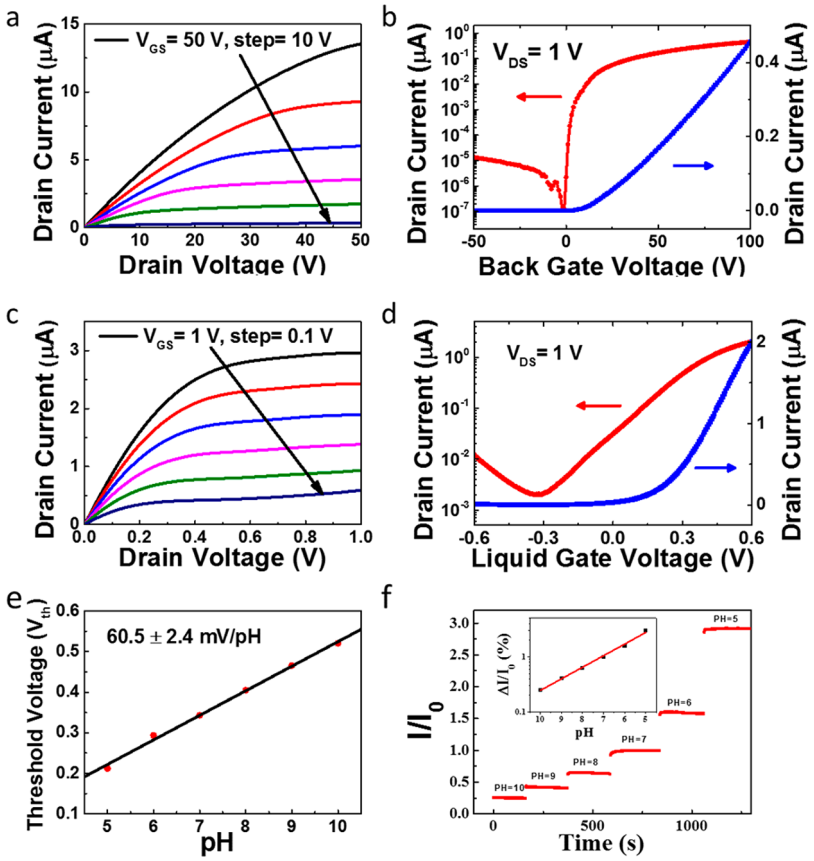

Figure 2. Electrical characterization of the In_2O_3 nanoribbon biosensor. (a) Family of I_{DS}−V_{DS} curves measured in ambient environment. Drain current as a function of drain voltage with the back gate voltage varying from 0 to 50 V in steps of 10 V. (b) Drain current *versus* back gate voltage with drain voltage fixed at 1 V. Current was plotted in logarithmic scale on the left axis and in linear scale on the right axis. (c) Family curves of I_{DS}−V_{DS} measured in 0.01× phosphate-buffered saline with the liquid gate varying from 1 to 0.5 V in steps of 0.1 V. (d) Drain current *versus* liquid gate voltage with drain voltage fixed at 1 V, also plotted in linear and logarithmic scale. (e) Change in threshold voltage with pH ranging from 5 to 10 and obtained with a pH sensitivity of ∼60.5 mV/pH. (f) Real-time responses obtained from an In_2O_3 nanoribbon device exposed to commercial buffer solutions with pH 5−10.

attaching the shadow mask onto the SiO_2/Si wafer. Then the In_2O_3 ribbons were deposited using radio frequency (RF) sputtering with a thickness ∼16 nm. We obtained well-defined nanoribbons by simply removing the shadow mask instead of lift-off as in photolithography. The source and drain electrodes were defined using the second shadow mask. After the alignment and attachment, we deposited 1 nm Ti and 50 nm Au using electron-beam evaporation. The whole process is photoresist-free, so it not only simplifies the fabrication process but also avoids the effect of any photoresist residue in the later sensing experiments. Figure 1b shows a photograph of 28 groups of In_2O_3 nanoribbon FETs patterned over a 3 in. wafer using shadow masks, and each group contains five FET devices (Figure 1c). Here, each chip has an array of sensors, so that we can use multiple devices in each round of biosensing to study the uniformity and consistency. In addition, biosensor arrays can be used for multiplex sensing to detect multiplexed antigens in one chip in the future. The scanning electron microscope (SEM) image of the channel regions (Figure 1d) shows that the nanoribbons are identical and have very clear edges. In this structure, the channel width and length were 25 and 500 μm, respectively. Furthermore, In_2O_3 nanoribbons are smooth, with 16 nm thickness (Figure 1e). Thickness is the key factor for sensitivity. In our previous work,[14] we demonstrated that the optimum thickness of the In_2O_3 nanoribbon should be within 23 nm (Debye length). Here, we obtained nanoribbon thickness of 16 nm, which is very close to the optimum thickness. The width and length of the channel are also believed to affect the sensitivity when they are comparable to the Debye length; however, such channel width and length are beyond what we can pattern with shadow masks.

The electrical characterization of the devices was first carried out in ambient environment by measuring the output and transfer characteristics as a function of drain and back gate voltages. Figure 2a,b shows family curves of drain current−drain voltage (I_{DS}−V_{DS}) and drain current−gate voltage (I_{DS}−V_{GS}) with drain voltage fixed at 1 V. High back gate voltage is required to turn on the device due to the presence of very thick back gate oxide. The output characteristics of the FET devices illustrate n-type transistor behavior with good saturation, and the In_2O_3 FETs show high field-effect mobilities (μ_{sat}) of 13.09 ± 1.39 $cm^2\ V^{-1}\ s^{-1}$ (averaged over 50 devices) and on/off ratios (I_{on}/I_{off}) above 10^7. The edge of devices fabricated using shadow masks is not as sharp as the edge of devices fabricated using photolithography. However, the shadow masks we used have small thickness of 125 μm and can be attached to the Si/SiO_2 wafer with no visible gap between. In addition, the sputtering system we use has a rather long working distance of ∼15 cm between the sputtering target and the substrate, making the "shadow" due to the edges of the shadow mask

DOI: 10.1021/acsnano.6b05171
ACS Nano XXXX, XXX, XXX−XXX

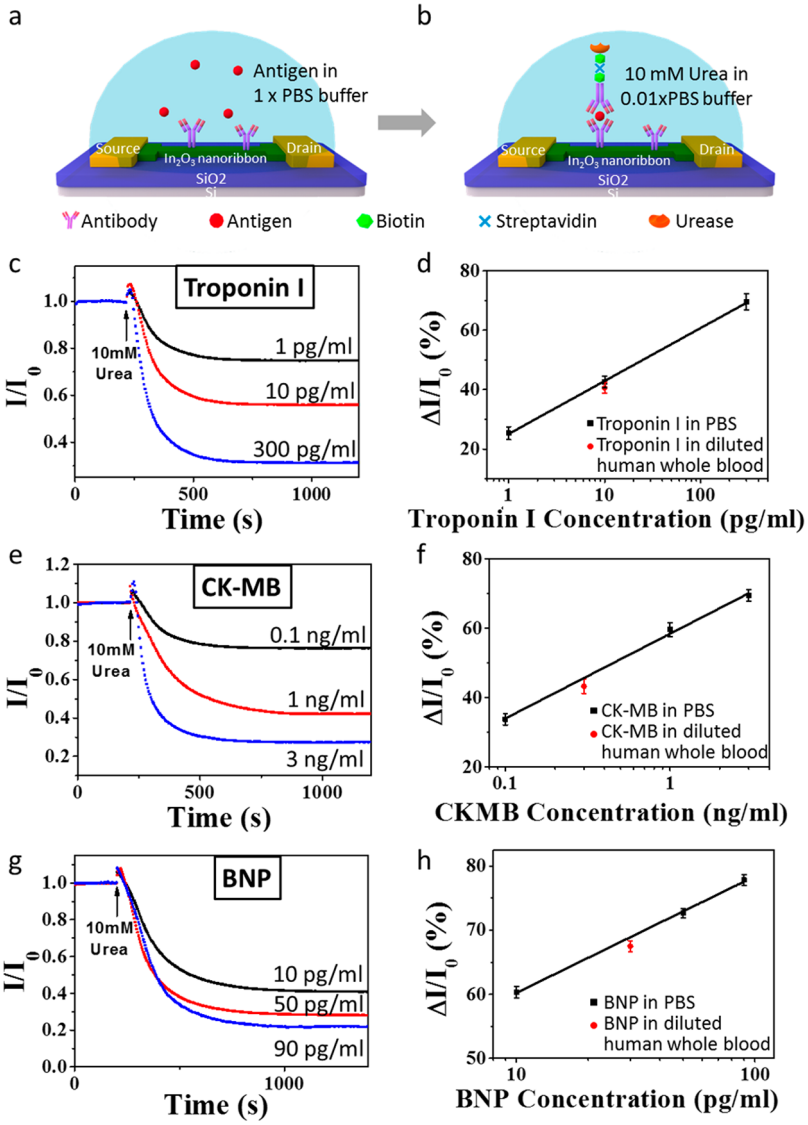

Figure 3. In_2O_3 nanoribbon biosensor and electronic ELISA for cardiac troponin I (cTnI), creatine kinase MB (CK-MB), and B-type natriuretic peptide (BNP) detection. (a) Schematic diagram of the antibodies capturing specific antigens in buffer solutions. (b) Schematic illustration of the electronic ELISA sensing setup. (c) Real-time sensing results of 1, 10, and 300 pg/mL of cTnI antigens in 1× PBS. (d) Average sensing results of three devices from three concentrations of cTnI proteins in 1× PBSr marked as a black square and one concentration of troponin I in diluted human whole blood marked as a red dot. Error bars represent standard deviations of three devices. (e) Real-time sensing results of 0.1, 1, and 3 ng/mL of CK-MB proteins in 1× PBS. (f) Average sensing responses from different concentrations of CK-MB. (g) Real-time responses of 10, 50, and 90 pg/mL of BNP proteins in 1× PBS. (h) BNP biomarker concentrations *versus* signal for three concentrations of BNP in 1× PBS and one concentration in diluted human whole blood.

almost negligible. We statistically analyzed 50 devices randomly selected from a wafer, and as the result shown in Figure S1, our devices showed very good uniformity, which is almost comparable to the uniformity of previous devices made using photolithography.

For biosensing applications, it is necessary that these devices can be operated in a wet environment. Hence, the devices were measured with the active channel materials immersed in a microwell filled with electrolyte solution (0.01× phosphate-buffered saline (PBS)). A Ag/AgCl reference electrode is used to apply bias to the electrolyte to stably operate the biosensor, which is referred to as a liquid gate. The performance of liquid-gated In_2O_3 FETs is shown in Figure 2c (I_{DS}–V_{DS}) and 2d (I_{DS}–V_{GS}). It illustrates that the biosensor device is efficiently controlled in the wet environment, and the In_2O_3 FETs have good FET behavior with saturation and low driving voltage.

In order to determine the pH sensitivity of the In_2O_3 FETs, we selected six devices randomly from the wafer, and recorded their response to pH solutions. The pH sensing is based on the protonation/deprotonation of the OH groups on the surface due to the pH of the electrolyte, and resultant changes in local FET electric fields, which cause changes in the conductance and current. The shift in threshold voltage was calculated using the extrapolation in the saturation region and found to be 60.5 ± 2.44 mV/pH at room temperature, close to the ideal result of 59.1 mV/pH at 25 °C.[27] Figure 2f shows the real-time sensing response of a nonfunctionalized In_2O_3 FET to standard pH calibration solutions. The initial current I_0 was obtained by using PBS to stabilize the device, and then the PBS was sequentially changed to commercial pH buffer solutions ranging from pH 10 to pH 5. The drain current responded quickly and log-linearly to each pH buffer.

DOI: 10.1021/acsnano.6b05171
ACS Nano XXXX, XXX, XXX–XXX

Direct electrical detection of biomolecules in their physiological environment is often impeded by the Debye screening from the high salt concentration in the sample solutions.[28] Sandwich enzyme-linked immunosorbent assay (ELISA), on the other hand, detects signals associated with the reactions between a test solution and the conjugated enzymes on secondary antibodies instead of the biomarker. The sandwiched structure not only overcomes the Debye screening from salts in the fluid but also incorporates an amplification scheme to improve the signal-to-noise ratio, which can be much higher than direct analyte detection without amplification, especially when the amount of analytes is small.

In the following In_2O_3 nanoribbon sensing experiments, we applied an electronic ELISA technique that uses pH change due to urease enzyme activities as the amplification signal. Figure 3a,b shows the schematic diagram depicting the electronic ELISA process. Prior to using In_2O_3 FET biosensors for biomarker detection, the surfaces were treated with phosphonic acid to confer phosphonic linker molecules to the indium oxide surface. Subsequently, we functionalized our devices with *N*-(3-dimethylaminopropyl)-*N*′-ethylcarbodiimide hydrochloride/*N*-hydroxysuccinimide (EDC/NHS) chemistry to immobilize the capture antibodies on the surface of In_2O_3 FETs, as mentioned in the Experimental Methods section and in our previous papers.[15,29,30] This was followed by a washing step that removed unbound capture antibodies (all binding steps described below were followed by three washes). A bovine serum albumin solution was used to prevent nonspecific protein adsorption to the chip and reservoir sidewalls, which is a typical blocking step used in conventional colorimetric ELISA protocols to minimize nonspecific binding.[31] This was followed by introducing known concentrations of the antigen-containing samples to the sensor for antigen−antibody binding (Figure 3a). The biomarkers were contained either within the physiological fluid sample of the patient or in a solution of buffer for experimental purposes. The biomarkers were subsequently captured by the antibodies, and any unbound ones were washed off. Next, a solution of biotinylated secondary antibodies, which are also specific to the cardiac biomarker, was introduced to the sensors using incubation, and the secondary antibodies bound to the biomarkers. After rinsing out unbound biotinylated antibody, we introduced streptavidin solution in PBS. The biotin end of the secondary antibody group was used to bind to a streptavidin, which in turn was bound to a biotinylated urease, the last solution to incubate the sensor.

When a solution of urea is introduced to the nanoribbon sensor surface with this sandwich structure, the urea causes an increase in the pH of the solution due to consumption of protons according to the following reaction.

$$\text{urea} + 2H_2O + H^+ \xrightarrow{\text{urease}} 2NH_4^+ + HCO_3^-$$

The urease reaction raises the pH of the solution, leading to deprotonation the surface hydroxyl groups on the In_2O_3 nanoribbon, ultimately lowering the surface potential. The increase in negative surface charges is responsible for the decrease in conduction of the n-type In_2O_3 nanoribbon FETs. The pH change is easily detected by the In_2O_3 nanoribbon sensors because the catalytic reaction promoted by urease amplifies the charge generated by the binding of the analyte by orders of magnitude over the direct binding between the antigens and the capture antibodies.[14,30] This amplifies the detection signal, allowing the sensor to detect very low concentrations of the antigen. Furthermore, the solution for the pH detection step is independent of the fluid containing the biomarker because the solutions are rinsed out after each step. This allows cardiac biomarkers to be collected in physiological samples such as whole blood without the limitation of the Debye screening effect, which complicates detection schemes based solely on direct binding between the antigens and the capture antibodies.[15]

Troponin, a Food and Drug Administrative approved biomarker for AMI, is the biomarker of choice for evaluating chest pain patients for possible heart attack. Troponin I and T are released into the bloodstream due to the death of cardiac muscle cells; therefore, troponin I and T are not present in the blood of healthy people. Elevated blood troponin levels have a positive correlation to the risk of death in the heart disease patients, and the biomarker is a good guide for identifying patients for certain types of treatment.[32,33] The 99th percentile of a reference decision limit (medical decision cutoff) for cardiac troponin (cTn) assays is over 40 pg/mL.[34] In the first biomarker detection experiment, we used troponin I as the model cardiac biomarker to demonstrate that the In_2O_3 nanoribbon biosensors can be used to optimize the electronic ELISA assay turnaround time by shortening the incubation of the cardiac biomarkers to 30 min in total. The incubation times of target analytes, biotinylated secondary antibodies, streptavidin, and biotinylated urease enzymes were 10, 10, 5, and 5 min, respectively.

We performed experiments with known concentration of cardiac troponin I (cTnI) in 1× PBS, namely, 1, 10, and 300 pg/mL, to build a standard curve covering the beginning of the second quartile for non-AMI patients to the median of AMI patients.[34] At time $t = 0$ in Figure 3c, the devices were rinsed with and submerged in 0.01× PBS when the baseline current was taken. The buffer was then replaced with 10 mM urea in 0.01× PBS at around 200 s as indicated by the arrow. It shows the real-time responses from three sensors when the urea solution was introduced into the sensing chamber that was previously incubated in 1, 10, and 300 pg/mL of cardiac troponin I (cTnI) in 100 μL of 1× PBS. The urease−urea interaction drastically reduces the device conductance by 25.3, 42.5, and 69.5% of the baseline signal, respectively. Figure 3d shows the average normalized responses for each cTnI concentration mentioned earlier. Each data point was calculated from three sensors monitored simultaneously during the experiment. The sensing response decreases exponentially upon the decrease in the concentration of cTnI target molecules. The current of the In_2O_3 nanoribbon sensor drops to about 42% of the baseline at a troponin concentration of 10 pg/mL and 25% at a concentration of 1 pg/mL. The sensitivity corresponds to about 17% conduction change per decade of biomarker concentration change. This is beneficial for covering a large range of concentrations for biomarkers such as cTnI, whose elevation in AMI patients is high. The pH changes between the buffer solutions used for the baseline and the final solutions in the sensing chamber were measured to be 0.17, 0.87, and 2.17 by a commercial Mettler Toledo pH meter. The averaged results were plotted in the Supporting Information (Figure S1). These increases in pH are consistent with the decreases in conduction of the In_2O_3 nanoribbon devices. Moreover, the total sample collection to result time is around 45 min, meeting the expectation of 1 h for practical use in diagnosis of myocardial infarction.

DOI: 10.1021/acsnano.6b05171
ACS Nano XXXX, XXX, XXX−XXX

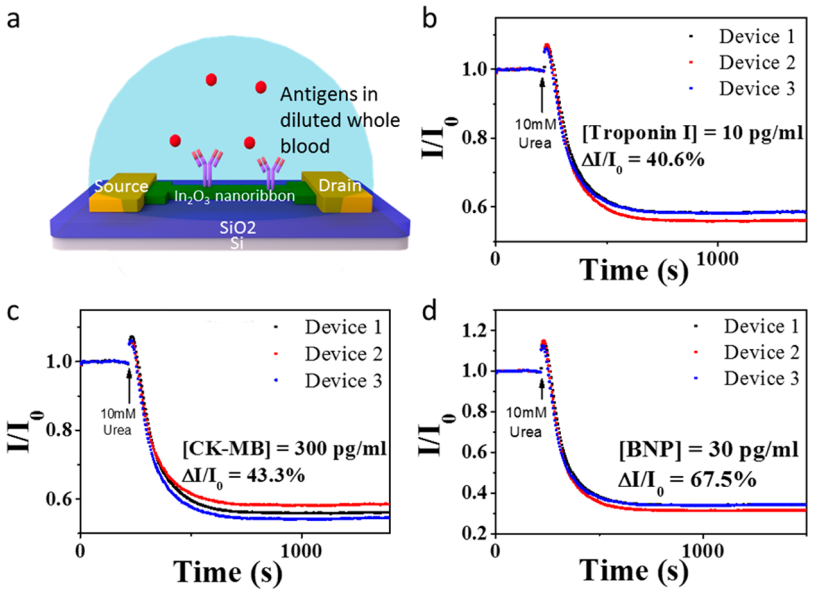

Figure 4. Real-time sensing results of cardiac biomarkers in diluted human whole blood. (a) Schematic diagram of antibodies that were anchored on the biosensor surfaces capturing specific biomarkers in diluted human whole blood. (b) Real-time sensing results of 10 pg/mL of cTnI in 10× diluted human whole blood, and the averaged results were plotted as a red dot in Figure 3d. (c) Real-time sensing results of 300 pg/mL of CK-MB in 10× diluted human whole blood, and the results were plotted as a red dot in Figure 3f. (d) Real-time sensing results of 30 pg/mL of BNP in 10× diluted human whole blood, and the results were plotted as a red dot in Figure 3h.

In addition to cTnI, the blood biomarker creatine kinase-MB (CK-MB) has long been used for AMI detection. Including the detection of CK-MB can improve early diagnosis of AMI because the level of CK-MB increases within 2−4 h after cardiac muscle injury.[35] The CK-MB level in the blood is relatively high compared to other biomarkers, with an interquartile range level of non-AMI patients at 0.6 to 1.7 ng/mL and that of AMI patients from 1.5 to 10.5 ng/mL.[35] Thus, the detection of CK-MB must be able to distinguish the concentration change less than 1 order of magnitude for effective diagnosis. We repeated the sensing for 0.1, 1, and 3 ng/mL, and the results are shown in Figure 3e, and the pH changes measured by a commercial pH meter are shown in Figure S2. Heart failure is strongly indicated when the blood sample has 30 ng/mL CK-MB before dilution or 3 ng/mL with 10× dilution. The average of data from three sensors for each concentration is plotted in Figure 3f with standard deviations plotted as the error bars. At 0.1 ng/mL, the current is ∼33% of the baseline, and at 1 ng/mL, the current is ∼60% of the baseline, yielding a difference equivalent to 27% of the baseline for a concentration difference of a decade. This large sensing response enables detection of minute changes in concentration, such as from 250 to 300 pg/mL or 2.5 to 3 ng/mL before 10× dilution. In addition, the small device-to-device signal standard deviation makes readout at this precision possible using the In_2O_3 nanoribbon sensor platform.

Beside cTnI and CK-MB, B-type natriuretic peptide (BNP) is also associated with heart failure and has been shown to substantially improve AMI diagnosis when included in a multiple cardiac biomarker panel.[36] More importantly, for blood samples taken when chest pain patients first arrive at the emergency department, BNP is shown to have quicker response for AMI diagnosis than other cardiac biomarkers such as CK-MB and troponin, which do not elevate until at least 2 h after the onset of AMI symptoms.[37] In fact, even when a patient's troponin level is normal, a BNP concentration greater than 100 pg/mL is a good indicator of AMI. BNP higher than 900 pg/mL is considered severe heart failure.[38] In order to simulate quantitative detection of BNP in patients' blood, we first obtained a standard calibration curve with known concentrations of BNP in buffer. As shown in Figure 3g, we have targeted BNP concentrations of 10, 50, and 90 pg/mL. For each of the three concentrations, three In_2O_3 nanoribbon sensors were used in the electronic ELISA assay as described in the previous sections. For the smallest concentration of 10 pg/mL, the current drops to ∼60% of the baseline after the introduction of 10 mM urea solution. For the 50 and 90 pg/mL detection, the current drops to 72 and 77% of the baseline, respectively. The average and the standard deviation for each of the three concentrations are plotted in Figure 3h, and the pH changes measured by a commercial pH meter are shown in Figure S3. We also performed the orthogonal tests for the three biomarkers to verify that our technology can distinguish these different biomarkers, and the results can be found in the Supporting Information.

Detection of cardiac biomarkers in whole blood is essential to POC sensor platforms used for situations where complicated patient blood processing is not possible and defeats the purpose of fast, cheap, and convenient disease testing. The main problems for FET sensor detection caused by whole blood are the nonspecific binding of nontarget proteins and the Debye length screening from salts. Recent efforts to process whole blood for FET sensors have been demonstrated using a microfluidic chip,[39] desalting columns,[40] and filtration.[15] In this work, we have made some improvements and demonstrated that by applying electronic ELISA assay on In_2O_3 nanoribbon sensors, we can detect cardiac biomarkers such as cTnI, CK-MB, and BNP in whole blood without any sample processing at all, as described below.

Cardiac biomarkers, cTnI, CK-MB, and BNP, are spiked with healthy human whole blood (purchased from Innovative Research) to simulate an AMI patient sample with a cTnI

DOI: 10.1021/acsnano.6b05171
ACS Nano XXXX, XXX, XXX−XXX

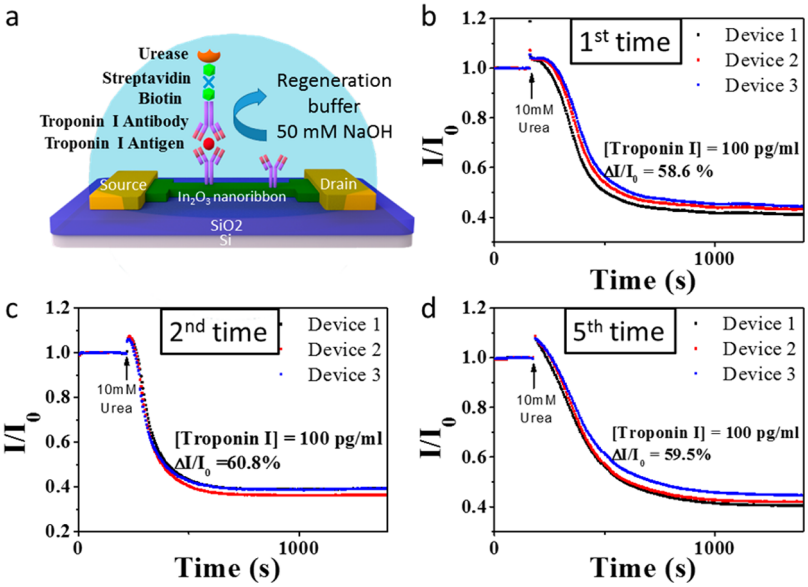

Figure 5. Reusability of In_2O_3 nanoribbon biosensors. (a) Schematic diagram of the regeneration process by applying 50 mM NaOH to the used sensor surface. After antibodies release antigens, the sensors are ready to repeat sensing. (b) Real-time responses of 100 pg/mL cTnI proteins in 1× PBS. (c) Real-time sensing responses from the same concentration of cTnI and the same devices after regeneration. (d) Real-time response of the same sensors after three more cycles of the regeneration and sensing process.

concentration of 100 pg/mL, a CK-MB concentration of 3 ng/mL, and a BNP concentration of 300 pg/mL, all indicating mild heart failure. Due to the fact that the human whole blood is very viscous, which may affect the sensing results, a real patient sample would be first diluted 10 times to be detected by the nanoribbon sensor. We note that this sample dilution is not due to the difficulties in ionic screening and does not filter out any nonspecific proteins or blood cells. To simulate this sample preparation, 100 μL of healthy whole blood was first diluted with 1× PBS to 930 μL. Then 10 μL of 1 ng/mL cTnI, 50 μL of 6 ng/mL CK-MB, and 10 μL of 3 ng/mL BNP in 1× PBS were added to the diluted whole blood to simulate 10 pg/mL cTnI, 0.3 ng/mL CK-MB, and 30 pg/mL BNP in 10× diluted whole blood. This sample was used to incubate the nanoribbon sensors prepared with capture antibodies, as shown in Figure 4a. The remaining steps of the electronic ELISA assay followed those described in previous sections. Figure 4b–d shows the real-time signal when 10 mM of urea in 0.01× PBS is introduced to each sensor. The current drop is 40.6% for 10 pg/mL cTnI, 43.3% for 0.3 ng/mL CK-MB, and 67.5% for 30 pg/mL BNP. In Figure 3d,f,h, the average responses of the three In_2O_3 nanoribbon sensors for this detection are placed on the calibration curve as red dots. The graph shows that the deviation of the detection signal from the calibration curve are all below 5%. This falls within the device-to-device variation and is expected for the experiment.

Because the cardiac biomarker concentrations are elevated in AMI patient, it is important for diagnosis and treatment to obtain the trend in the cardiac biomarker concentration in the hours after the patient's arrival. The reusability of the In_2O_3 nanobiosensor can give results every hour when the sensing is repeated. What's more, the reusability of the biosensors is also cost-effective. Following the regeneration process of antibodies and antigens,[41] we applied 50 mM NaOH as regeneration buffer (from GE Healthcare) to a sensor that had already been used for cTnI biomarker sensing. As shown in Figure 5a, when the sensors are rinsed with washing buffer, the proteins will antibond the capture antibody. After being rinsed with 1× PBS, the proteins will all be washed away, leaving the antibody still active and bonded to the surface of the sensor. To demonstrate that the sensors can still work well after being washed, we start from incubation with samples containing cTnI biomarkers and repeated the electronic ELISA process as before. Figure 5b–d shows the sensing results for the first time, the second time, and the fifth time, respectively. They all fall around 60%, indicating that the regeneration process can efficiently wash proteins away and leave sufficient capture antibodies for reusability.

We note that while this paper focuses on In_2O_3 nanoribbon sensors, our approach is not limited to In_2O_3 and can be applied to many other materials, such as other kinds of semiconducting metal oxides, as long as the semiconducting material can be deposited through a shadow mask, including InGaZnO, ZnO, InN,[42,43] and SnO_2. In our previous work,[14] we studied several possible materials, such as In_2O_3, InGaZnO, SnO_2, ZnO, and tin-doped indium oxide (ITO). In the study,[14] InGaZnO and SnO_2 showed higher resistance, higher threshold voltage, and lower on/off ratio than the In_2O_3 samples; ITO showed poor gate dependence, and ZnO showed poor stability in an aqueous environment. CdO, NiO, and other possible materials may also be suitable to work as channel materials, which need further investigation.

In a production setting, further improvements can be made for even better uniformity by monitoring the nanoribbon film thickness after sputtering and chemical modification to reduce the device-to-device variation down a fraction of a percentage. Such highly uniform batches of sensors can give good statistical confidence for their reported biomarker concentrations. This confidence level combined with a turnaround time of 45 min is a good basis for improving current POC devices for cardiac marker detection in an emergency situation. Moreover, the platform can be integrated with other electronic components for better data analysis.

DOI: 10.1021/acsnano.6b05171
ACS Nano XXXX, XXX, XXX–XXX

CONCLUSIONS

In conclusion, we have demonstrated the fabrication of highly uniform and scalable In_2O_3 nanoribbon biosensor chips using two simple shadow masks to define the position and dimension of metal electrodes and nanoribbons, and the devices have shown outstanding performance. Furthermore, In_2O_3 nanoribbon devices show good electrical performance in the aqueous condition when gate voltage is applied through the liquid gate electrode. In addition, the In_2O_3 nanoribbon devices show good performance in a pH sensing experiment with change in conduction by a factor of 12 when pH is reduced from 10 to 5. Through all the sensing experiments, we have demonstrated that In_2O_3 nanoribbon biosensors fabricated by shadow masks can be used to quantitatively detect three cardiac biomarkers within the concentrations relevant to clinical diagnosis with the turnaround time of ∼45 min. We further demonstrated tests using spiked cardiac biomarkers in diluted human whole blood, with results consistent with the calibration curve established using PBS. Lastly, by applying a regeneration buffer to the used sensor surfaces to antibond the antigen−antibody conjugation and repeating the sensing experiments, we demonstrated the reusability of the In_2O_3 nanoribbon biosensors with very small variation of each sensing results.

EXPERIMENTAL METHODS

Materials. A 3 in. 500 nm SiO_2 on Si wafers was purchased from SQI. Au and Ti for metal sources of electron-beam evaporation and an indium oxide (In_2O_3) sputtering target with purity of 99.99% were obtained from Plasmaterials. 3-Phosphonopropioninc acid with a purity of 94%, EDC with a purity of 98%, and NHS with a purity of 98% were purchased from Sigma-Aldrich. Shadow masks for patterning were purchased from Photo Science. Troponin I monoclonal antibodies, troponin I proteins, biotinylated troponin I monoclonal antibodies, CK-MB antibodies, CK-MB proteins, biotinylated CK-MB antibodies, BNP antibodies, and BNP proteins were purchased from Fitzgerald Industries. Biotinylated BNP polyclonal antibodies were purchased from Abcam.

Shadow Mask Fabrication Method. A SiO_2/Si wafer was rinsed with acetone and isopropyl alcohol before being dried in a nitrogen stream before the fabrication process. After solvent cleaning, the SiO_2/Si substrate was placed on a hot plate at 120 °C for 5 min to repel all solvent residual and cooled in room temperature. After the cleaning process, the first shadow mask was attached to the SiO_2/Si wafer to pattern the channel area. Then the In_2O_3 ribbons were deposited by RF sputtering (by Denton Discovery 550 sputtering system in NRF). By simply removing the shadow mask, we obtained well-defined nanoribbons. The source and drain electrodes were defined by the second shadow mask. After using an aligner to pattern the source and drain area, we attached the shadow mask and the substrate. Deposition followed with 1 nm Ti and 50 nm Au by employing electron-beam evaporation. After deposition, the shadow mask was removed and yielded a pristine surface.

Characterization. Optical microscopy images were taken with Olympus microscope. Atomic force microscopy imaging was performed on a Digital Instruments DI 3100 under tapping mode. The SEM images were taken with a Hitachi S-4800 field-emission scanning electron microscope. Electrical characteristics of the In_2O_3 TFTs were measured with an Agilent 4156B Precision semiconductor parameter analyzer in ambient environment. Electrical characteristics in a wet environment and sensing results were measured with an Agilent 1500B semiconductor analyzer.

ASSOCIATED CONTENT

Supporting Information

The Supporting Information is available free of charge on the ACS Publications website at DOI: 10.1021/acsnano.6b05171.

Additional experimental details and Figures S1−S7 (PDF)

AUTHOR INFORMATION

Corresponding Authors

*E-mail: chongwuz@usc.edu.
*E-mail: met@usc.edu.

Notes

The authors declare no competing financial interest.

ACKNOWLEDGMENTS

The authors acknowledge financial support from the Ming Hsieh Institute.

REFERENCES

(1) Nourjah, P. National Hospital Ambulatory Medical Care Survey: 1997 Emergency Department Summary. *Advance Data from Vital and Health Statistics* **1999**, *304*, 1−24.

(2) Gibler, B. W.; Young, G. P.; Hedges, J. R.; Lewis, L. M.; Smith, M. S.; Carleton, S. C.; Aghababian, R. V.; Jorden, R. O.; Jackson, A. E.; Often, E. J.; et al. Acute Myocardial Infarction in Chest Pain Patients with Nondiagnostic Ecgs: Serial CK-MB Sampling in the Emergency Department. *Annals of Emergency Medicine* **1992**, *21*, 504−512.

(3) Brush, J. E., Jr; Brand, D. A.; Acampora, D.; Chalmer, B.; Wackers, F. J. Use of the Initial Electrocardiogram to Predict in-Hospital Complications of Acute Myocardial Infarction. *N. Engl. J. Med.* **1985**, *312*, 1137−1141.

(4) Lee, T. H.; Rouan, G. W.; Weisberg, M. C.; Brand, D. A.; Cook, E. F.; Acampora, D.; Goldman, L. Sensitivity of Routine Clinical Criteria for Diagnosing Myocardial Infarction within 24 h of Hospitalization. *Ann. Intern. Med.* **1987**, *106*, 181−6.

(5) Rude, R. E.; Poole, W. K.; Muller, J. E.; Turi, Z.; Rutherford, J.; Parker, C.; Roberts, R.; Raabe, D. S.; Gold, H. K.; Stone, P. H.; Willerson, J. T.; Braunwald, E. Electrocardiographic and Clinical-Criteria for Recognition of Acute Myocardial-Infarction Based on Analysis of 3,697 Patients. *Am. J. Cardiol.* **1983**, *52*, 936−941.

(6) Braunwald, E.; Antman, E. M.; Beasley, J. W.; Califf, R. M.; Cheitlin, M. D.; Hochman, J. S.; Jones, R. H.; Kereiakes, D.; Kupersmith, J.; Levin, T. N.; Pepine, C. J.; Schaeffer, J. W.; Smith, E. E., 3rd; Steward, D. E.; Theroux, P.; Gibbons, R. J.; Alpert, J. S.; Eagle, K. A.; Faxon, D. P.; Fuster, V.; et al. Acc/Aha Guidelines for the Management of Patients with Unstable Angina and Non-St-Segment Elevation Myocardial Infarction: Executive Summary and Recommendations. A Report of the American College of Cardiology/American Heart Association Task Force on Practice Guidelines (Committee on the Management of Patients with Unstable Angina). *Circulation* **2000**, *102*, 1193−209.

(7) Ng, S. M.; Krishnaswamy, P.; Morissey, R.; Clopton, P.; Fitzgerald, R.; Maisel, A. S. Ninety-Minute Accelerated Critical Pathway for Chest Pain Evaluation. *Am. J. Cardiol.* **2001**, *88*, 611−617.

(8) Lewandrowski, K.; Chen, A.; Januzzi, J. Cardiac Markers for Myocardial Infarction. A Brief Review. *Pathol. Patterns Rev.* **2002**, *118* (Suppl), S93.

(9) Han, J. H.; Gibler, W. B. Biomarkers in the Emergency Department: Rapid Diagnosis and Triage. In *Cardiovascular Biomarkers: Pathophysiology and Disease Management*; Morrow, D. A., Ed.; Humana Press: Totowa, NJ, 2006; pp 61−77.

(10) Wu, A. H. B.; Apple, F. S.; Gibler, W. B.; Jesse, R. L.; Warshaw, M. M.; Valdes, R. National Academy of Clinical Biochemistry Standards of Laboratory Practice: Recommendations for the Use of Cardiac Markers in Coronary Artery Diseases. *Clin. Chem.* **1999**, *45*, 1104−1121.

(11) Lewandrowski, E.; Januzzi, J. L., Jr.; Grisson, R.; Mohammed, A. A.; Lewandrowski, G.; Lewandrowski, K. Evaluation of First-Draw Whole Blood, Point-of-Care Cardiac Markers in the Context of the Universal Definition of Myocardial Infarction: A Comparison of a

DOI: 10.1021/acsnano.6b05171
ACS Nano XXXX, XXX, XXX−XXX

Multimarker Panel to Troponin Alone and to Testing in the Central Laboratory. *Arch. Pathol. Lab. Med.* **2011**, *135*, 459−63.
(12) Mu, L.; Droujinine, I. A.; Rajan, N. K.; Sawtelle, S. D.; Reed, M. A. Direct, Rapid, and Label-Free Detection of Enzyme−Substrate Interactions in Physiological Buffers Using Cmos-Compatible Nanoribbon Sensors. *Nano Lett.* **2014**, *14*, 5315−5322.
(13) Kong, T.; Su, R.; Zhang, B.; Zhang, Q.; Cheng, G. Cmos-Compatible, Label-Free Silicon-Nanowire Biosensors to Detect Cardiac Troponin I for Acute Myocardial Infarction Diagnosis. *Biosens. Bioelectron.* **2012**, *34*, 267−272.
(14) Aroonyadet, N.; Wang, X.; Song, Y.; Chen, H.; Cote, R. J.; Thompson, M. E.; Datar, R. H.; Zhou, C. Highly Scalable, Uniform, and Sensitive Biosensors Based on Top-Down Indium Oxide Nanoribbons and Electronic Enzyme-Linked Immunosorbent Assay. *Nano Lett.* **2015**, *15*, 1943−1951.
(15) Chang, H.-K.; Ishikawa, F. N.; Zhang, R.; Datar, R.; Cote, R. J.; Thompson, M. E.; Zhou, C. Rapid, Label-Free, Electrical Whole Blood Bioassay Based on Nanobiosensor Systems. *ACS Nano* **2011**, *5*, 9883−9891.
(16) Kim, J.; Rim, Y. S.; Chen, H.; Cao, H. H.; Nakatsuka, N.; Hinton, H. L.; Zhao, C.; Andrews, A. M.; Yang, Y.; Weiss, P. S. Fabrication of High-Performance Ultrathin In_2O_3 Film Field-Effect Transistors and Biosensors Using Chemical Lift-Off Lithography. *ACS Nano* **2015**, *9*, 4572−4582.
(17) Li, C.; Lei, B.; Zhang, D.; Liu, X.; Han, S.; Tang, T.; Rouhanizadeh, M.; Hsiai, T.; Zhou, C. Chemical Gating of In_2O_3 Nanowires by Organic and Biomolecules. *Appl. Phys. Lett.* **2003**, *83*, 4014−4016.
(18) Lei, B.; Li, C.; Zhang, D.; Zhou, Q.; Shung, K.; Zhou, C. Nanowire Transistors with Ferroelectric Gate Dielectrics: Enhanced Performance and Memory Effects. *Appl. Phys. Lett.* **2004**, *84*, 4553−4555.
(19) Gao, W.; Emaminejad, S.; Nyein, H. Y. Y.; Challa, S.; Chen, K.; Peck, A.; Fahad, H. M.; Ota, H.; Shiraki, H.; Kiriya, D.; et al. Fully Integrated Wearable Sensor Arrays for Multiplexed *in Situ* Perspiration Analysis. *Nature* **2016**, *529*, 509−514.
(20) Cui, Y.; Wei, Q.; Park, H.; Lieber, C. M. Nanowire Nanosensors for Highly Sensitive and Selective Detection of Biological and Chemical Species. *Science* **2001**, *293*, 1289−1292.
(21) Goldsmith, B. R.; Mitala, J. J.; Josue, J.; Castro, A.; Lerner, M. B.; Bayburt, T. H.; Khamis, S. M.; Jones, R. A.; Brand, J. G.; Sligar, S. G.; Luetje, C. W.; Gelperin, A.; Rhodes, P. A.; Discher, B. M.; Johnson, A. T. C. Biomimetic Chemical Sensors Using Nanoelectronic Readout of Olfactory Receptor Proteins. *ACS Nano* **2011**, *5*, 5408−5416.
(22) Chen, P. C.; Sukcharoenchoke, S.; Ryu, K.; Gomez de Arco, L.; Badmaev, A.; Wang, C.; Zhou, C. 2, 4, 6-Trinitrotoluene (Tnt) Chemical Sensing Based on Aligned Single-Walled Carbon Nanotubes and Zno Nanowires. *Adv. Mater.* **2010**, *22*, 1900−1904.
(23) Naylor, C. H.; Kybert, N. J.; Schneier, C.; Xi, J.; Romero, G.; Saven, J. G.; Liu, R.; Johnson, A. T. C. Scalable Production of Molybdenum Disulfide-Based Biosensors. *ACS Nano* **2016**, *10*, 6173−6179.
(24) Star, A.; Gabriel, J.-C. P.; Bradley, K.; Grüner, G. Electronic Detection of Specific Protein Binding Using Nanotube Fet Devices. *Nano Lett.* **2003**, *3*, 459−463.
(25) Zheng, G.; Patolsky, F.; Cui, Y.; Wang, W. U.; Lieber, C. M. Multiplexed Electrical Detection of Cancer Markers with Nanowire Sensor Arrays. *Nat. Biotechnol.* **2005**, *23*, 1294−1301.
(26) Chen, R. J.; Bangsaruntip, S.; Drouvalakis, K. A.; Kam, N. W. S.; Shim, M.; Li, Y.; Kim, W.; Utz, P. J.; Dai, H. Noncovalent Functionalization of Carbon Nanotubes for Highly Specific Electronic Biosensors. *Proc. Natl. Acad. Sci. U. S. A.* **2003**, *100*, 4984−4989.
(27) Sarkar, D.; Liu, W.; Xie, X.; Anselmo, A. C.; Mitragotri, S.; Banerjee, K. Mos_2 Field-Effect Transistor for Next-Generation Label-Free Biosensors. *ACS Nano* **2014**, *8*, 3992−4003.
(28) Butler, J. E. Enzyme-Linked Immunosorbent Assay. *J. Immunoassay* **2000**, *21*, 165−209.
(29) Li, C.; Curreli, M.; Lin, H.; Lei, B.; Ishikawa, F. N.; Datar, R.; Cote, R. J.; Thompson, M. E.; Zhou, C. Complementary Detection of Prostate-Specific Antigen Using In_2O_3 Nanowires and Carbon Nanotubes. *J. Am. Chem. Soc.* **2005**, *127*, 12484−5.
(30) Stern, E.; Vacic, A.; Li, C.; Ishikawa, F. N.; Zhou, C.; Reed, M. A.; Fahmy, T. M. A Nanoelectronic Enzyme-Linked Immunosorbent Assay for Detection of Proteins in Physiological Solutions. *Small* **2010**, *6*, 232−8.
(31) Hermanson, G. T. *Bioconjugate Techniques*; Academic Press: New York, 2013.
(32) Newby, L. K.; Christenson, R. H.; Ohman, E. M.; Armstrong, P. W.; Thompson, T. D.; Lee, K. L.; Hamm, C. W.; Katus, H. A.; Cianciolo, C.; Granger, C. B.; Topol, E. J.; Califf, R. M. Investigators, G.-I., Value of Serial Troponin T Measures for Early and Late Risk Stratification in Patients with Acute Coronary Syndromes. *Circulation* **1998**, *98*, 1853−1859.
(33) Ohman, E. M.; Armstrong, P. W.; Christenson, R. H.; Granger, C. B.; Katus, H. A.; Hamm, C. W.; O'Hanesian, M. A.; Wagner, G. S.; Kleiman, N. S.; Harrell, F. E.; Califf, R. M.; Topol, E. J.; et al. Cardiac Troponin T Levels for Risk Stratification in Acute Myocardial Ischemia. *N. Engl. J. Med.* **1996**, *335*, 1333−1342.
(34) Mahajan, V. S.; Jarolim, P. How to Interpret Elevated Cardiac Troponin Levels. *Circulation* **2011**, *124*, 2350−2354.
(35) Saenger, A. K.; Jaffe, A. S. Requiem for a Heavyweight the Demise of Creatine Kinase-MB. *Circulation* **2008**, *118*, 2200−2206.
(36) Christenson, R. H.; Azzazy, H. M. E. Biomarkers of Myocardial Necrosis. In *Cardiovascular Biomarkers: Pathophysiology and Disease Management*; Morrow, D. A., Ed.; Humana Press: Totowa, NJ, 2006; pp 3−25.
(37) Bassan, R.; Potsch, A.; Maisel, A.; Tura, B.; Villacorta, H.; Nogueira, M. V.; Campos, A.; Gamarski, R.; Masetto, A. C.; Moutinho, M. A. B-Type Natriuretic Peptide: A Novel Early Blood Marker of Acute Myocardial Infarction in Patients with Chest Pain and No St Segment Elevation. *Eur. Heart J.* **2005**, *26*, 234−240.
(38) Morrison, L. K.; Harrison, A.; Krishnaswamy, P.; Kazanegra, R.; Clopton, P.; Maisel, A. Utility of a Rapid B-Natriuretic Peptide Assay in Differentiating Congestive Heart Failure from Lung Disease in Patients Presenting with Dyspnea. *J. Am. Coll. Cardiol.* **2002**, *39*, 202−209.
(39) Stern, E.; Vacic, A.; Rajan, N. K.; Criscione, J. M.; Park, J.; Ilic, B. R.; Mooney, D. J.; Reed, M. A.; Fahmy, T. M. Label-Free Biomarker Detection from Whole Blood. *Nat. Nanotechnol.* **2010**, *5*, 138−42.
(40) Zheng, G. F.; Patolsky, F.; Cui, Y.; Wang, W. U.; Lieber, C. M. Multiplexed Electrical Detection of Cancer Markers with Nanowire Sensor Arrays. *Nat. Biotechnol.* **2005**, *23*, 1294−1301.
(41) Duan, X.; Li, Y.; Rajan, N. K.; Routenberg, D. A.; Modis, Y.; Reed, M. A. Quantification of the Affinities and Kinetics of Protein Interactions Using Silicon Nanowire Biosensors. *Nat. Nanotechnol.* **2012**, *7*, 401−407.
(42) Cai, X.-M.; Hao, Y.-Q.; Zhang, D.-P.; Fan, P. Direct Current Magnetron Sputtering Deposition of Inn Thin Films. *Appl. Surf. Sci.* **2009**, *256*, 43−45.
(43) Tang, T.; Han, S.; Jin, W.; Liu, X.; Li, C.; Zhang, D.; Zhou, C.; Chen, B.; Han, J.; Meyyapan, M. Synthesis and Characterization of Single-Crystal Indium Nitride Nanowires. *J. Mater. Res.* **2004**, *19*, 423−426.

DOI: 10.1021/acsnano.6b05171
ACS Nano XXXX, XXX, XXX−XXX